Anal. Bioanal. Electrochem., Vol. 8, No. 2, 2016, 193-206

Analytical & Bioanalytical Electrochemistry

2016 by CEE
www.abechem.com

Full Paper

Electrochemical Preparation and Characterization of Porous Nanostructured Mn_3O_4 with Excellent Supercapacitive Performance

Ramin Cheraghali [1,*] and Mustafa Aghazadeh [2]

[1]*Chemistry Department, Saveh Branch, Islamic Azad University, Saveh, Iran*
[2]*Nuclear Science and Research Institute (NSTIR), Tehran, Iran*

*Corresponding Author, Tel.: +98-21-82064289; Fax: +98-21-82064289
E-Mail: Ramincheraghali@yahoo.com, Mustafa.aghazadeh@gmail.com

Received: 21 December 2015 / Accepted: 1 February 2016 /
Published online: 31 March 2016

Abstract- Porous nanostructured Mn_3O_4 was deposited from 0.005 M manganese nitrate bath using a one-pot cathodic electrodeposition route. The deposition experiments were performed under the direct current mode with applying a current density of 10 mA cm^{-2}. The structural analyses by XRD and FTIR, revealed that the product is composed of pure tetragonal Mn_3O_4. Morphological observation by SEM and TEM disclosed that the prepared Mn_3O_4 product is made up of porous plates at nanoscale. BET analysis further revealed that the prepared sample has high surface are of 125 m^2/g with mesoporous structure. Electrochemical evaluations by cyclic voltammetry and charge-discharge tests also showed the prepared Mn_3O_4 to be capable of delivering high specific capacitance values of 328 F g^{-1}, in addition to exhibiting excellent long-term cycling stability (95.9% of initial capacity after discharging 1000 cycles).

Keywords- Mn_3O_4, Pulse electrodeposition, Porous structure, Supercapacitors

1. INTRODACTION

Supercapacitors are currently subject as an energy storage device due to their high power density, good rate performance and long cycling life. They are playing an increasingly

important role in various applications ranging from portable electronics to hybrid electric vehicles. They are usually defined into electrochemical double layer capacitors (EDLCs) and pseudo-capacitors based on their different energy storage mechanisms. Generally, the carbon based porous materials, including graphene, activated carbon and carbon nanotubes (CNTs) that offer high surface areas and readily accessible mesopores are widely used for EDLCs, where the charge storage process is non-Faradic and energy storage is electrostatic [1]. At the same time, the capacitance of the pseudocapacitors is mainly from Faradic redox reaction. Their electrode materials generally involve various metal oxides [2] and conductive polymers [3]. In recent years, transition metal oxides have been drawn extensive research attentions for pseudo-capacitors since they could provide higher capacitance than carbon materials and longer cycle life than conductive polymers [4]. Recently, considerable efforts have been dedicated to identifying inexpensive electrode materials with acceptable capacitive performances. In this regard, transitions metal oxides have been extensively investigated as an electrode material for high performance supercapacitors due to their higher capacitance than carbon materials, and better cycling stability than conductive polymers [5].

Manganese oxides (MnO_2, Mn_3O_4 and MnO) are important materials that exhibit excellent properties required for achieving high capacitance [6–9]. Among these compounds, Mn_3O_4 is a potentially interesting material for use in supercapacitors due to its low cost, environmental benignity and relatively broad applicable potential window in aqueous solutions [10-12]. However, it has been subject relatively less investigation as compared with MnO_2 compounds. Mn_3O_4 plays important roles in elemental biogeochemical cycles [13], electrode materials [14,15], catalysts [16,17] and soft magnetic materials [18] etc.

In general, Mn_3O_4 is prepared by heating manganese oxides or manganese hydroxides, oxyhydroxide, nitrate, sulfate and carbonate at about 1000 ^oC in air. Other methods including co-precipitation [19,20], sol–gel technique [21], reverse-micellar precipitation [22], thermal decomposition [23–25], templating processes [26], polyol-mediated [27], chelation-mediated synthesis [28] and hydrothermal/solvothermal synthesis [29–32] have been employed to prepare Mn_3O_4 particles. Unfortunately most of these methods are hazardous due to the use of solvents and reducing agents therein. In the light of the increased awareness about environmental pollution, more emphasis has been directed towards identifying alternative synthesis pathways based on green chemistry methods. So, the evaluation of simple, low-temperature solution-based synthesis routes for the production of Mn_3O_4 nanostructures is a worthy endeavor by far. In this regards, electrodeposition methods can present attractive routes for the preparation of nanostructured Mn_3O_4 [33–38]. The most significant advantage of such methods is being clean and inexpensive, as well as providing it's the potential to manipulate the structural and morphological properties of the deposited films through manipulation of parameters such as current density, potential, concentration, pH, temperature, nature of the surfactant and substrate type [39,40]. However, these methods further require a

thermal annealing step which is necessary for converting the as-deposited Mn hydroxide to Mn oxide. In fact, the prepared deposit should be thermally treated to obtain the final oxide product.

A novel finding in this paper is the preparation of Mn_3O_4 via one-step cathodic electrodeposition. In fact, we found that the cathodic electrodeposition of Mn_3O_4 from a nitrate bath under the mild conditions, leads to the formation of Mn_3O_4 nanoplates. It was further found under these conditions the need for the presence of an O_2 atmosphere which was required in previously reported route [37] is eliminated. According to the overall procedure of the current work a galvanostatic cathodic deposition (i=10 mA cm^{-2}) procedure was performed in a 0.005 M nitrate bath at bath temperature of 60 ^oC leading to the production of pure Mn_3O_4 deposit with porous structures in the absence of templates, surfactants and a thermal-treatment step. Further, the electrochemical properties of the prepared Mn_3O_4 were investigated by cyclic voltammetry and galvanostatic charge–discharge measurements, which resulted that the obtained Mn_3O_4 porous structures have excellent supercapacitive performances i.e. high specific capacitance and long cycle life.

2. EXPERIMENTAL SECTION

2.1. Chemicals

$Mn(NO_3)_2$.$6H_2O$ (Merck), polytetrafluoroethylene (PTFE, Merck), carbon black and Na_2SO_4 (Merck) were used as received. All solutions were prepared using water purified by a UHQ Elga System. An aqueous solution of 0.005 M $Mn(NO_3)_2$.$6H_2O$ was prepared for electrodeposition.

2.2. Preparation of Mn_3O_4 sample

Nanostructured Mn_3O_4 was prepared through a one-step process electrodeposition from nitrate bath under a direct current (DC) mode with applying a current density of 10 mA cm^{-2} (I=10 mA cm^{-2}). The deposition time and bath temperature were 15 min and 60^oC, respectively. Prior to each deposition, the steel substrates were galvanostatically electropolished. The deposition experiments were conducted using an electrochemical workstation system (Potentiostat/Galvanostat, Model: NCF-PGS 2012, Iran). After the deposition, the steel substrates were repeatedly rinsed with water and then dried at 40 ^oC for 5h. Finally the deposits were scraped from the substrates and evaluated by further analyses.

2.3. Characterization

The phase composition and structure of the prepared samples were assessed through powder X-ray diffraction (XRD) on a Phillips PW-1800 diffractometer with a Cu Kα

radiation source in 2θ values ranging from 10 to 70 °C at a scanning rate of 5 degree/min. FTIR spectra of the samples were obtained using a Bruker Vector 22 Fourier transformed infrared spectroscope, in the range of 400–4000 cm^{-1} at ambient temperature, with samples in a KBr wafer. Each FTIR spectrum was acquired after 20 scans at a resolution of 4 cm^{-1} from 400 to 4000 cm^{-1}. BET specific surface area measurements were carried out based on the nitrogen adsorption data in a relative pressure range from 0.05 to 0.98, employing a Quanta-chrome NOVA-2200e system. The average distribution of the pore sizes was calculated using the BJH method. All of the adsorption and desorption isotherms were obtained at –196ºC. Prior to each measurement, the sample was degassed under vacuum at 110 °C for 5 h. The morphologies of the prepared Mn_3O_4 powder was studied using a scanning electron microscope (SEM, LEO 1455 VP, Oxford, UK, operating voltage 30 kV). Transmission electron microscopy (TEM) images were also acquired using a Phillips EM 208 transmission electron microscope with an accelerating voltage of 100 kV.

2.4. Electrochemical measurements

The Mn_3O_4 working electrodes were fabricated by mixing the prepared Mn_3O_4 powder (85 wt.%), carbon black (10 wt.%) and polytetrafluorene ethylene (PTFE, 5 wt.%). Next a small amount of ethanol was added to the mixture to produce a homogeneous paste. The mixture was then pressed onto steel grid current collectors to form the working electrodes. The electrochemical characterizations, suing these electrodes, were carried out in a conventional three electrode cell with a 1 M Na_2SO_4 as the electrolyte. A platinum foil and an Ag/AgCl (saturated with 1 M KCl) electrode were used as the counter and reference electrodes, respectively. All electrochemical measurements were conducted on an electrochemical workstation system (AUTOLAB®, Eco Chemie, PGSTAT 30). The cyclic voltammetric studies (CV) were conducted in a potential range of between -0.1 and 0.85 V versus Ag/AgCl at various scan rates of 2, 5, 10, 25, 50 and 100 mV s^{-1}. The constant current charge–discharge tests were carried out at different current densities of 0.5, 1, 2, 5 and 10 A g^{-1} within a potential range of 0 to 0.85 V versus Ag/AgCl reference electrode.

3. RESUITS AND DISCUSSION

3.1. Structural characterization of the prepared sample

The XRD pattern of the prepared sample is shown in Fig. 1. All the observed diffraction peaks in this pattern can be indexed to the Mn_3O_4 reference data (JCPDS card of 011-127, space group of $I4_1/amd$, a_0=5.75 Å, c_0=9.42 Å). FT-IR analysis was also recorded in the wavelength range of 400-4000 cm^{-1}. Fig. 2 shows FT-IR spectrum of the prepared sample. The spectrum shows an absorbance pattern which is similar to those of Mn_3O_4 obtained in previous studies [41-43]. The band at 3429 cm^{-1} was attributed to stretching vibration of -OH,

and the bands at 1038 and 981 cm^{-1} are usually attributed to bending vibrations of –OH bound with Mn atoms [42]. The peaks in the range of 400-700 cm^{-1} were indicative of the existence of octahedral MnO6 [43]. The bond located at 622 cm^{-1} is characteristic of Mn–O stretching modes in tetrahedral sites whereas the vibration frequency located at 514 cm^{-1} relates to the distortion vibrations of Mn–O in octahedral ones. The third band located at 419 cm^{-1} is indicative of the vibration of manganese species (Mn^{3+}–O) in the octahedral sites of Mn_3O_4 [41,42]. Notably, a sharp peak at 1383 cm^{-1} in the IR spectra (Fig. 2) is assigned to the vibration modes of NO_3^- anions intercalated in the deposit structure during the deposition process [37-40].

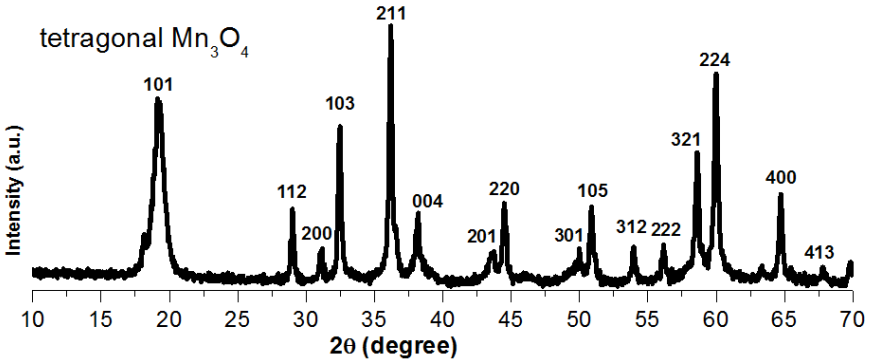

Fig. 1. XRD pattern of the deposited Mn_3O_4 sample

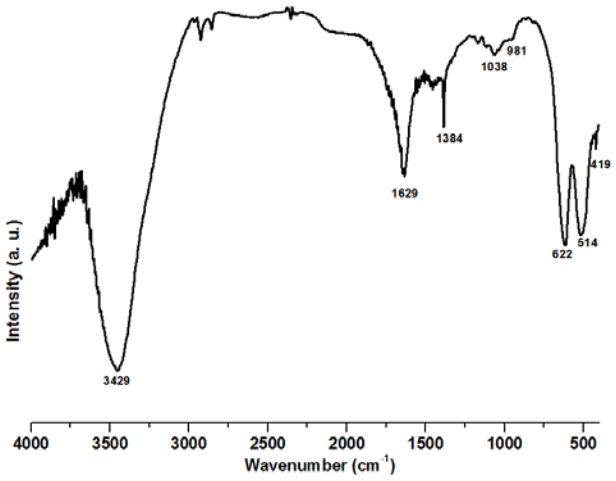

Fig. 2. IR spectrum of the deposited Mn_3O_4 sample

3.2. Morphological characterization of the prepared Mn_3O_4

Morphological characteristics of the prepared Mn_3O_4 sample are shown in Fig. 3. The SEM image in Fig. 3a reveals that the majority of the prepared Mn_3O_4 sample has plate-like

structures. It was seen that the sample has plate morphology and almost all of plates have porous texture. Furthermore, there are voids between the Mn_3O_4 plates so that it can be said that the prepared sample has porous structure. High magnification by TEM clearly showed that the Mn_3O_4 plates have porous texture. They were approximately 100 nm in length and have a thin diameter (Fig. 3b). These characteristics of the prepared sample make it to exhibit large surface area and better supercapacitive performance.

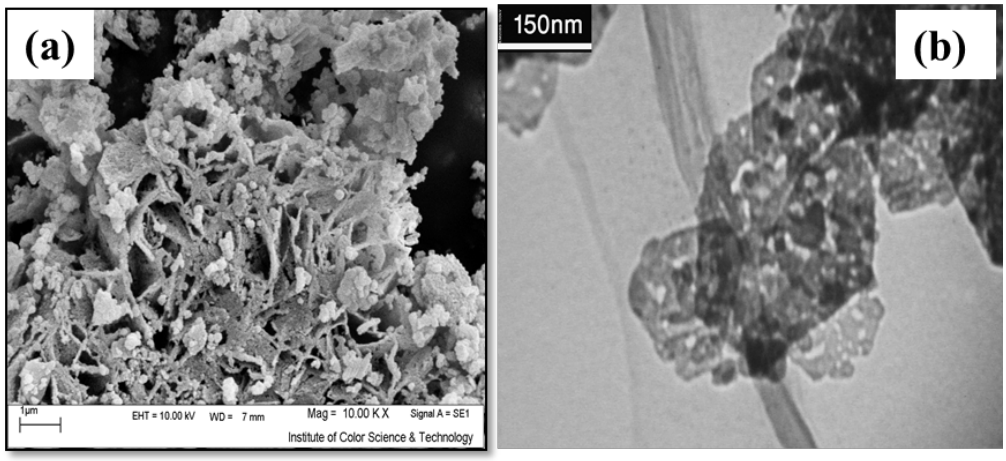

Fig. 3. (a) SEM and (b) TEM images of the prepared Mn_3O_4

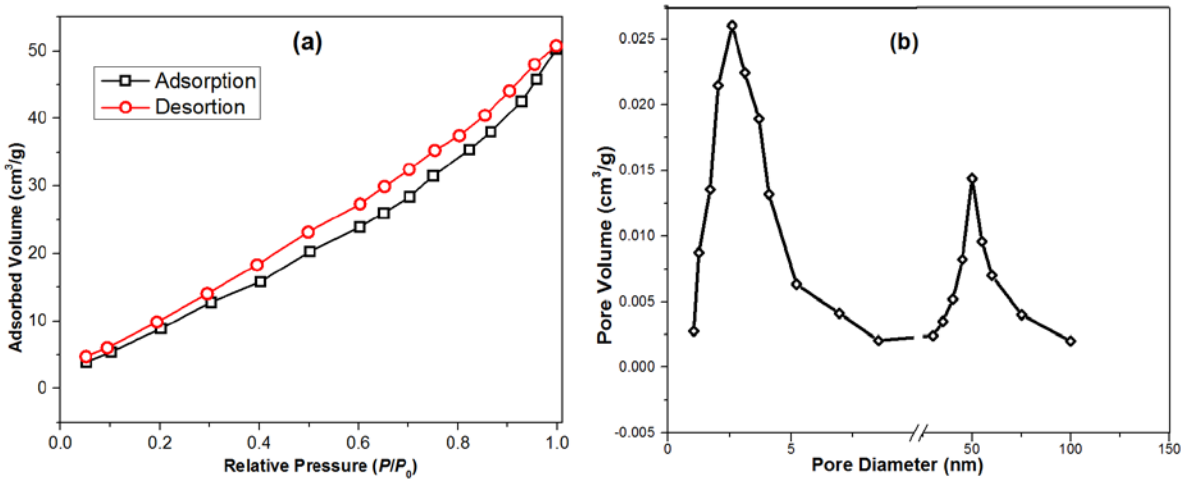

Fig. 4. (a) N_2 adsorption–desorption isotherms and (b) the BJH pore-size distribution curve of the prepared Mn_3O_4 sample

3.3. Surface area

The surface area of the Mn_3O_4 product was measured using the Brunauer–Emmett–Teller (BET) method. Representative N_2 desorption/adsorption isotherms and the corresponding

BJH (Barret-Joyner-Halenda) pore size distribution curve of the Co_3O_4 nanoplates are shown in Fig. 4. The N_2 isotherm of Mn_3O_4 nanoplates has a type II form with a large type H4 hysteresis loop, indicating the presence of microporous materials according to the IUPAC classification [44]. The H4 loop, which does not exhibit any limiting adsorption, is indicating the high ratio of porous Mn_3O_4 plates. The H4 loop is also observed with aggregates of Mn_3O_4 plates giving rise to slit-shaped pores. The Mn_3O_4 nanoplates have a high BET surface area of 125 m^2 g^{-1}. The pore size distribution, as calculated by the BJH method from the desorption branch of the nitrogen isotherm, revealed that the nanoplates contain small mesoporous with a pore size of 4.3 nm and large mesoporous with a pore size of about 55 nm (Fig. 4b). The former mesoporous exist among small primary Mn_3O_4 nanoparticles in the nanoplates. The latter textural mesoporous are formed as a result of the removal of structural water and nitrate ions during the heat treatment, which is in agreement with TEM observations (Fig. 3b), and also aggregation of the thin nanoplates during testing.

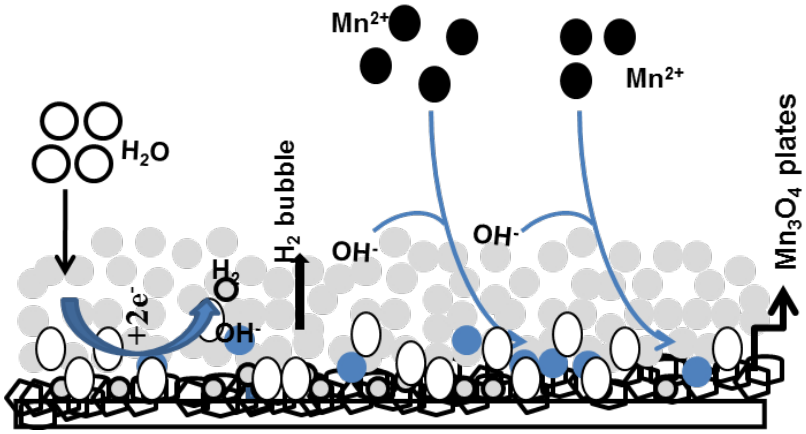

Fig. 5. Schematic illustration of cathodic electrodeposition of Mn_3O_4

3.4. Mechanism of Mn_3O_4 formation

A schematic view of the electrochemical and chemical steps in the cathodic electrodeposition of Mn_3O_4 is shown in Fig. 5. Formation of the Mn_3O_4 deposit on the cathode surface from the chloride bath can be described on the basis of a two–step electrochemical–chemical (EC) mechanism [35-37]:

- The electrochemical step:

$O_2+2H_2O+4e^- \rightarrow 4OH^-$ $E^o=+0.26$ V *vs.* Ag/AgCl (1)

$2H_2O+2e^- \rightarrow H_2+2OH^-$ $E^o=-1.08$ V *vs.* Ag/AgCl (2)

The above reactions result in an increase of the pH near the steel electrode surface. By increasing the OH^- concentration, Mn_3O_4 particles form and deposit on the cathode electrode:

- The chemical step:

$$3Mn^{2+}(aq)+ 6OH^{-}(aq) + 1/2O_2 \rightarrow Mn_3O_4 +3H_2O \quad (3)$$

Considering the value of the applied potential (-1.15 V *vs.* Ag/AgCl) during the deposition process, the reduction of water (reaction (2) was expected to have a major role in the electrogeneration of base at the applied conditions. In fact, the electrochemical step precedes reactions (2), during the deposition process as schematically shown in Fig. 5. Once the pH of the solution reaches a required value, Mn_3O_4 molecules are formed near the cathode surface (Fig. 5). The H_2 gas bubbles can affect the surface morphology of the deposit and also act as a dynamic template for the formation and the growth of Mn_3O_4 deposit [37-39].

3.5. Electrochemical evaluation

The electrochemical performance of the prepared Mn_3O_4 electrodes, were evaluated by cyclic voltammetry (CV) and galvanostatic charge-discharge measurements in a three electrode system. Cyclic voltammograms (CVs) of Mn_3O_4 were recorded between -0.1 and 0.85 V *vs*. Ag/AgCl at various scan rates (2–100 mV s^{-1}) and the results are shown in Fig. 6a. There were no specific redox peaks in the CVs of Mn_3O_4 electrodes, which confirmed that the charge and discharge process of the Mn_3O_4 electrode is on the base of pseudocapacitance performance.

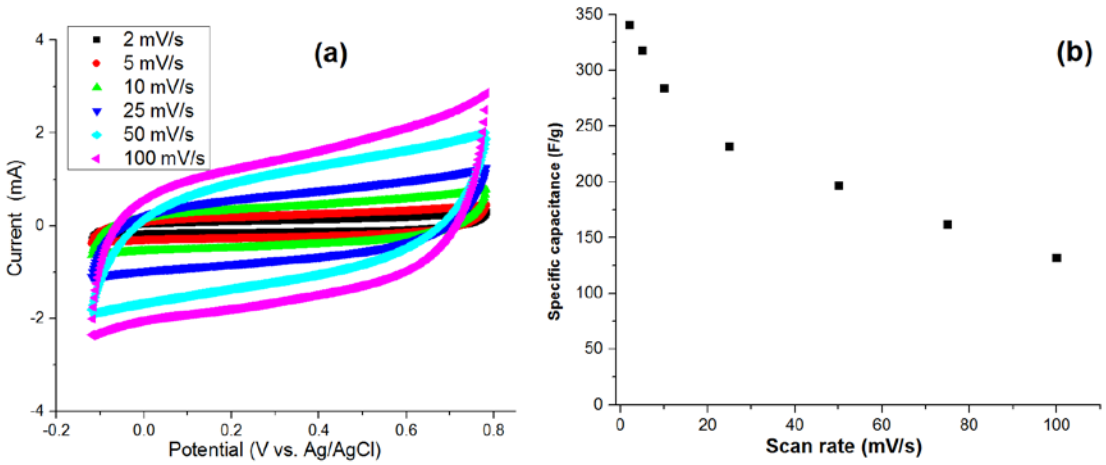

Fig. 6. (a) Cyclic voltammograms of the Mn_3O_4 electrode at various scan rates of 2, 5, 10, 25, 50 and 100 mV s^{-1}, and (b) the calculated specific capacitances from CV curves

All CVs were close to rectangular in shape, which is indicative of the behavior of an ideal capacitor. These results revealed good electrochemical reversibility and an ideally capacitive

behavior [46], which may be attributed to the nanoscale and porous texture of Mn_3O_4 plates (as seen in TEM image; Fig. 3b). Nano size, porous texture and plate-like arrangement of the Mn_3O_4 can greatly reduce the diffusion length, over which Na^+ must transfer during the charge/discharge process, providing the better electrochemical utilization of Mn_3O_4 [47].

All CVs were close to rectangular in shape, which is indicative of the behavior of an ideal capacitor. These results revealed good electrochemical reversibility and an ideally capacitive behavior [46], which may be attributed to the nanoscale and porous texture of Mn_3O_4 plates (as seen in TEM image; Fig. 3b). Nano size, porous texture and plate-like arrangement of the Mn_3O_4 can greatly reduce the diffusion length, over which Na^+ must transfer during the charge/discharge process, providing the better electrochemical utilization of Mn_3O_4 [47].

The specific capacitance values of the Mn_3O_4 electrode was determined by integrating the area of the CV curves as follows:

$$C = \frac{1}{m\vartheta(\Delta V)} \int_{V_A}^{V_C} I(V)dV \quad (1)$$

Where C is the specific capacitance (F g^{-1}), ΔV is the potential range (0.95 V), *m* is the mass of Mn_3O_4 (g), *v* is the scan rate (V s^{-1}), and I(V) is the current response. Using Eq. (1), specific capacitances of 341, 318, 284, 232, 197 and 142 F g^{-1} were calculated at scan rates of 2, 5, 10, 25, 50 and 100 mV s^{-1}, respectively (Fig. 6b). These values indicated the excellent supercapacitive performance of the prepared porous Mn_3O_4 nanoplates. The charging–discharging mechanism of Mn_3O_4 electrode in Na_2SO_4 aqueous solution is mainly governed by the insertion and/or release of Na^+ from the electrolyte into the Mn_3O_4 nanoplates and/or from the Mn_3O_4 nanoplates into the electrolyte. The charge storage in spinal Mn_3O_4, in presence of Na_2SO_4 can be expressed as follows [48,49]:

$$Mn_3O_4 \text{ (spinel)} \rightarrow Na_\delta MnO_x.nH_2O \text{ (birnessite)} \quad (4)$$

$$Na_\delta MnO_x.nH_2O + yH^+ + zNa^+(y+Z)e^- \leftrightarrow Na_{\delta+z}MnO_x.nH_2O \quad (5)$$

Increasing the scan rate has a direct impact on the diffusion of Na^+ into the Mn_3O_4 material. At low scan rates (e.g. 2 mV s^{-1}), Na^+ from the electrolyte can easily diffuse into almost all available electrode material, leading to a complete insertion reaction, and showing an almost ideal capacitive behavior, as well as a high specific capacitance value of 318 F g^{-1}. However, increasing the scan rate had a direct impact on the diffusion of Na^+ into the Mn_3O_4 plates and also the observed capacitance behavior. At high scan rates (e.g. 100 mV s^{-1}), Na^+ can only approach the outer surface of the electrode and some porous plates, and due to the considerable reduction of effective interactions among the ions and the electrode, the capacity loss is relatively high (Fig. 6b). However, the prepared Mn_3O_4 nanoplates showed specific capacitance values of 142 F g^{-1} at the high scan rate of 100 mV s^{-1}, which confirmed their good electrochemical performance.

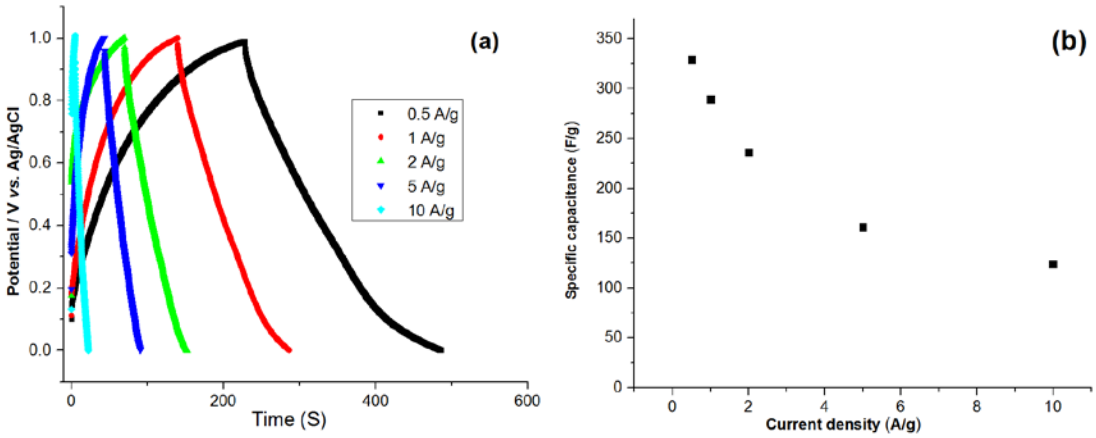

Fig. 7. (a) Charge-discharge profiles of Mn_3O_4 electrode at different applied current densities and (b) the calculated specific capacities at the applied current densities

The galvanostatic charge-discharge technique is a reliable method for the evaluation of the supercapacitive performance of prepared electrode. Fig. 7 shows the charge–discharge profiles of Mn_3O_4 nanoplates at the current densities of 0.5, 1, 2, 5 and 10 A g^{-1}. The Mn_3O_4 electrode is observed to have a stable electrochemical performance in the 1 M Na_2SO_4 electrolyte, based on the good linear variation of potential versus time observed for all the curves. This behavior is a typical characteristic of an ideal capacitor. Almost no voltage drop is observed during the discharge process, which can be due to the high capacity of the electrode material. The specific capacitance (SC) of the Mn_3O_4 electrode can be calculated according to the following equation:

$$\boldsymbol{C = \frac{I \times \Delta t}{m \times \Delta V}} \qquad (2)$$

Where I is the applied constant current (A), *m* is the mass of Mn_3O_4, ΔV is the potential window during cycling and Δt is the time of a cycle (s).

Using Eq. (2), and based on the calculations, it was found that the produced Mn_3O_4 particles are capable of delivering capacitances as high as 338, 301, 257, 161 and 124 F g^{-1} at the applied current densities of 0.5, 1, 2, 5 and 10 A g^{-1}, respectively (Fig. 7). These values confirmed the excellent electrochemical performance of the prepared electrode. Also the capacitance values calculated from the charge-discharge curves are in agreements with the calculated ones from the CVs (Fig. 6b). Furthermore, the observed capacitances were comparable with those reported for nanostructured Mn_3O_4 prepared by deposition methods so far (e.g. 293 and 240 F g^{-1} at the scan rate of 10 mV s^{-1} for RuO_2/Mn_3O_4 and Mn_3O_4 electrodes prepared by electrospinning [9], 223 F g^{-1} at 5 mV s^{-1} for Mn_3O_4 electrode prepared by chemical bath deposition [15], 330 F g^{-1} at 20 mV s^{-1} for MnO_x films prepared by cathodic deposition [30], 235.4 F g^{-1} at 10 mV s^{-1} for Mn_3O_4 nanospheres prepared by

cathodic deposition [33] and 322 F g^{-1} at the current density of 0.5 mA cm^{-2} for Mn_3O_4 nanoparticles prepared by chemical precipitation [41]).

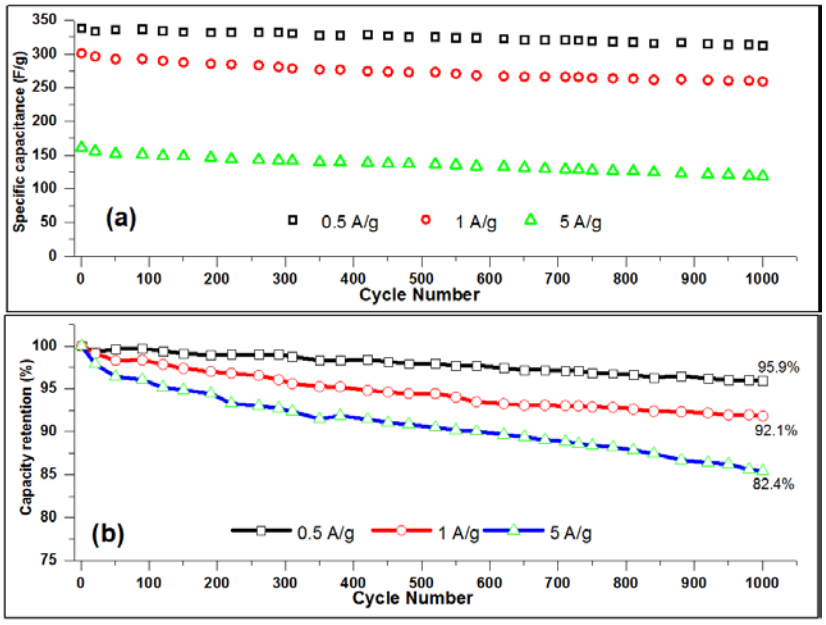

Fig. 8. Supercapacitive performance of Mn_3O_4 electrode at the applied current densities of 0.5, 1 and 5 A g^{-1} during 1000 cycles; (a) specific capacitance and (b) capacity retention *vs*. cycle number

To investigate the cyclability of the Mn_3O_4 electrode, the working electrodes prepared using Mn_3O_4 nanoplates were cycled (1000 cycling) at the applied current densities of 0.5, 1 and 5 A g^{-1}, respectively. Fig. 8 shows the performance i.e. specific capacitance and cycle life of the Mn_3O_4 nanorods. The specific capacitance values of each cycle, at the applied scan rate were calculated using Eq. (2) and the results are shown in Fig. 8a. Also based on the obtained capacitance values, the capacity retention of the MnO_2 nanobelts on cycling was evaluated (Fig. 8b). As can be seen in Fig. 8b, the prepared electrode showed capacity retentions of 95.9%, 92.1% and 82.4% at the applied current densities of 0.5, 1 and 5 A g^{-1}, respectively. These results confirmed the excellent supercapacitive performance of the prepared Mn_3O_4.

4. CONCLUSION

Mn_3O_4 nanoplates were deposited through a simple one-pot galvanostatic cathodic electrosynthesis procedure not requiring a thermal treatment step. The electrochemical evaluations by cyclic voltammetry and charge-discharge techniques revealed that the electrodeposited Mn_3O_4 nanostructures were capable to deliver high capacitance and stable capacity retentions. The specific capacitances as high as 338, 301, 257, 161 and 124 F g^{-1} at the applied current densities of 0.5, 1, 2, 5 and 10 A g^{-1}, respectively. The excellent cycling

stabilities of 95.9%, 92.1% and 82.4% after 1000 cycles were also observed at the applied current densities of 0.5, 1 and 5 A g^{-1}, respectively. The Mn_3O_4 nanoplates were found to have a high potential for use as the electrode material in supercapacitors.

REFERENCES

[1] Y. Wu, S. Liu, H. Wang, X. Wang, X. Zhang, and G. Jin, Electrochim. Acta 90 (2013) 210.

[2] C. D. Lokhande, D. P. Dubal, and O. S. Joo, Curr. Appl. Phys. 11 (2011) 255.

[3] R. J. Shabani Shayeh, A. Ehsani, M. R. Ganjali, P. Norouzi, and B. Jaleh, Appl. Surf. Sci. 353 (2015) 594.

[4] J. Shabani Shayeh, A. Ehsani, A. Nikkar, P. Norouzi, M. R. Ganjaliad, and M. Wojdyla, New J. Chem. 39 (2015) 9454.

[5] M. Aghazadeh, J. Appl. Electrochem. 42 (2012) 89.

[6] M. Aghazadeh, M.G. Maragheh, M.R. Ganjali, P. Norouzi, and F. Faridbod, Appl. Surf. Sci. 364 (2016) 141.

[7] J. Tizfahm, M. Aghazadeh, M.G. Maragheh, M.R. Ganjali, and P Norouzi, Mater. Lett. 167 (2016) 153.

[8] H. Abe, T. Tanimoto, and M. Nakayama, J. Electrochem. Soc. 162 (2015) A1952.

[9] M. Aghazadeh, M. Asadi, M.G. Maragheh, M.R. Ganjali, and P. Norouzi, Appl. Surf. Sci. 364 (2016) 726.

[10] X. She, X. Zhang, J. Liu, L. Li, X. Yu, Z. Huang, and S. Shang, Mater. Res. Bulletin 70 (2015) 945.

[11] M. Aghazadeh, M.G. Maragheh, M.R. Ganjali, and P. Norouzi, RSC Adv. 6 (2016) 10442.

[12] J. G. Wang, F. Kang, and B. Wei, Prog. Mater. Sci. 74 (2015) 51.

[13] M. R. Ganjali, R. Kiani-Anbouhi, M. Shamsipur, T. Poursaberi, M. Salavati-Niasari, Z. Talebpour, M. Emami, Electroanalysis 16 (2004) 1002.

[14] Y. Xiao, Y. Cao, Y. Gong, A. Zhang, J. Zhao, S. Fang, D. Jia, and F. Li, J. Power Sour. 246 (2014) 926.

[15] C. L. Liu, K. H. Chang, C. C. Hu, and W. C. Wen, J. Power Sour. 217 (2012) 184.

[16] Y. Li, J. Qu, F. Gao, S. Lv, L. Shi, C. He, and J. Sun, Appl. Catal. B: Environmental 162 (2015) 268.

[17] M. Liu, Y. Wang, Z. Cheng, M. Zhang, M. Hu, and J. Li, Appl. Surf. Sci. 313 (2014) 360.

[18] H. W. Kim, Y. J. Kwon, H. G. Na, H. Y. Cho, C. Lee, and J. H. Jung, Microelect. Eng. 139 (2015) 60.

[19] H.Y. Xu, S. Xu, H. Wang, and H. Yan, J. Electrochem. Soc. 152 (2005) C803.

[20] D. P. Dubal, D. S. Dhawale, R. R. Salunkhe, S. M. Pawar, and C. D. Lokhande, Appl. Surf. Sci. 256 (2010) 4411.
[21] M. Anilkumar, and V. Ravi, Mater. Res. Bull. 40 (2005) 605.
[22] T. Ahmad, K. V. Ramanujachary, S. E. Lofland, and A. K. Ganguli, J. Mater. Chem. 14 (2004) 3406.
[23] D. S. Wang, T. Xie, Q. Peng, S. Y. Zhang, J. Chen, and Y. D. Li, Chem. Eur. J. 14 (2008) 2507.
[24] F. Davar, M. Salavati-Niasari, N. Mir, K. Saberyan, M. Monemzadeh, and E. Ahmadi, Polyhedron 29 (2010) 1747.
[25] W. Z. Wang, and L. Ao, Cryst. Growth Des. 8 (2008) 358.
[26] C. Du, J. Yun, R. K. Dumas, X. Yuan, K. Liu, N. D. Browning, and N. Pan, Acta Mater. 56 (2008) 3516.
[27] T. Rhadfi, J. Y. Piquemal, L. Sicard, F. Herbst, E. Briot, M. Benedetti, A. Atlamsani, App. Catal. A: General 386 (2010) 132.
[28] C. Feldmann, Solid State Sci. 7 (2005) 868.
[29] L. X. Yang, Y. Liang, H. Chen, Y. F. Meng, and W. Jiang, Mater. Res. Bull. 44 (2009) 1753.
[30] Y. Wu, S. Liu, H. Wang, X. Wang, X. Zhang, and G. Jin, Electrochim. Acta 90 (2013) 210.
[31] L. Kuang, R. Dong, Z. Zhang, L. Feng, F. Wang, and Y. Wen, Mater. Res. Bull. 48 (2013) 3122.
[32] Y. Liu, Z. F. Gao, Q. Sun, and Y. P. Zeng, Solid State Sci. 14 (2012) 1462.
[33] C. C. Hu, C. Y. Hung, K. H. Chang, and Y. L. Yang, J. Power Sour. 196 (2011) 847.
[34] N. Nagarajan, H. Humadi, and I. Zhitomirsky, Electrochim. Acta 51 (2006) 3039.
[35] N. Nagarajan, M. Cheong, and I. Zhitomirsky, Mater. Chem. Phys. 103 (2007) 47.
[36] J. A. Koza, I. P. Schroen, M. M. Willmering, and J. A. Switzer, Chem. Mater. 26 (2014) 4425.
[37] T. Yousefi, A. Nozad Golikand, M. H. Mashhadizadeh, and M. Aghazadeh, J. Taiwan Inst. Chem. Eng. 43 (2012) 614.
[38] T. Yousefi, A. Nozad Golikand, M. H. Mashhadizadeh, and M. Aghazadeh, Curr. Appl. Phys. 12 (2012) 544.
[39] M. Aghazadeh, A. A. Malek Barmi, H. Mohammad Shiri, and S. Sedaghat, Ceram. Int. 39 (2013)1045.
[40] M. Aghazadeh, and M. Hosseinifard, Ceram. Int. 39 (2013) 4427.
[41] M. Ishii, M. Nakahira, T. Yamanaka, Solid State Commun. 11 (1972) 209.
[42] W. Z. Wang, C. K. Xu, G.H. Wang, Y. K. Liu, and C. L. Zheng, Adv. Mater. 14 (2002) 837.

[43] N. Gupta, A. Verma, S. C. Kashyap, and D. C. Dube, J. Magn. Magnet. Mater. 308 (2007) 137.
[44] F. Rouquerol, J. Rouquerol, and K. Sing, Adsorption by powders and porous solids: principles, methodology and applications, Academic Press, San Diego (1999).
[45] G. J. Soler-Illia, C. Sanchez, B. Lebeau, and J. Patarin, Chem. Rev. 102 (2002) 4093.
[46] C. C. Hu, and T. W. Tsou, Electrochem. Commun. 4 (2002) 105.
[47] J. Yan, Z.J. Fan, T. Wei, W. Z. Qian, M. L. Zhang, and F. Wei, Carbon 48 (2010) 3825.
[48] B. Gnana Sundara Raj, A. M. Asiri, J. J. Wu, and S. Anandan, J. Alloys Compd. 636 (2015) 234.
[49] J. Yang, X. Yang, Y.L. Zhong, and J. Y. Ying, Nano Energy 13 (2015) 702.